Optics and Lasers in Engineering 74 (2015) 80–86

Contents lists available at ScienceDirect

Optics and Lasers in Engineering

journal homepage: www.elsevier.com/locate/optlaseng

A carrier removal technique for Fourier transform profilometry based on principal component analysis

Shijie Feng, Qian Chen, Chao Zuo*, Jiasong Sun, Tianyang Tao, Yan Hu

Jiangsu Key Laboratory of Spectral Imaging & Intelligent Sense, Nanjing University of Science and Technology, Nanjing, Jiangsu Province 210094, China

ARTICLE INFO

Article history:
Received 10 November 2014
Received in revised form
25 April 2015
Accepted 19 May 2015
Available online 11 June 2015

Keywords:
Fringe projection
Dynamic scenes
Fourier transform profilometry
Principal component analysis

ABSTRACT

We present a carrier removal method for Fourier transform profilometry using the principal component analysis. The proposed approach is able to decompose the phase map into several principal components, in which the phase of the carrier can be extracted from the first dominant component acquired. It can cope well with the nonlinear carrier problem resulted from the divergent illumination which is commonly adopted in the fringe projection profilometry. It is effective, fully automatic and does not require the estimation for system geometrical parameters or the prior knowledge on the measured object. Further, the influence of the lens distortion is considered thus the carrier can be determined more accurately. The principle of the technique is verified by our experiments, showing that it performs well in both static and dynamic measurements.

1. Introduction

Fringe projection profilometry has been widely employed for shape measurement in recent years [1–4]. In a generalized fringe projection system, a fringe pattern is projected to the measured object and from another view a camera is used to capture the pattern modulated by the object surface. Then the profile can be retrieved through a fringe analysis method. There are a number of techniques to analyze the captured fringe pattern and generally they can be categorized into two classes. The first class based on the phase-shifting algorithm always requires at least three fringe patterns to reconstruct a 3D profile [5–7]. By contrast, the second class dependant on Fourier transform needs only one frame to retrieve the contour of a measured scene [8–11]. With the rapid advance in the digital projection and imaging system, more and more interests have been attached to the surface measurement of moving or deforming object [12–15]. Because the Fourier transform profilometry (FTP) is insensitive to the movement or deformation, it has been adopted extensively in dynamic measurements. In FTP, through Fourier transform, filtering and inverse Fourier transform, a phase map including object phase and carrier phase is obtained. To retrieve the object phase from the map, it is necessary to remove the unwanted carrier phase.

To deal with the issue of the carrier, a number of approaches have been developed. Takeda et al. [16] suggested that the carrier can be removed by a spectral translation in frequency domain because a spectrum shift of f is equivalent to a phase subtraction of $2\pi f$ in spatial domain. It is easy to be implemented and is robust if the captured stripes are equally spaced. However, for a generalized fringe projection set-up, the light beam is cast divergently onto the measured object which results in unequally distributed fringes across the measured scene. Therefore, a constant spectrum shift f will be insufficient to eliminate the variant (nonlinear) carrier. Thus to cope with this issue, in their following work they proposed a method [17] that requires respective measurements of the object and the reference plane. Then the effect of the carrier can be eliminated by subtracting the reference from the object phase map. Although this method is robust, it requires two measurements thus may be not very convenient to be implemented. After that, Chen et al. [18,19] developed a technique in which a polynomial function is used to describe the nonlinear carrier. Then Zhang et al. [20] presented a similar approach using the Zernike polynomials to represent the carrier. Both of the methods can effectively address the nonlinear carrier issue. However, in these two techniques data points need to be selected from the reference plane for the estimation of the polynomial coefficients, thus increasing human interventions.

Recently, in the field of digital holography, Zuo et al. [21] employed the principal component analysis (PCA) to compensate the phase aberration. Here, we introduce the PCA into our work aiming at removing the carrier in FTP for the divergent illumination measuring system. As aforementioned, the spectral translation enables the elimination of the linear carrier and retains the nonlinear one. In our method, thus, the PCA is carried out to study the remaining nonlinear carrier phase. We find that the first

* Corresponding author.
E-mail addresses: geniusshijie@163.com (S. Feng), chenq@njust.edu.cn (Q. Chen), surpasszuo@163.com (C. Zuo).

http://dx.doi.org/10.1016/j.optlaseng.2015.05.009
0143-8166/

dominant component of the exponential form of the phase map can describe the concerned nonlinear carrier phase. Therefore, we extract the first dominant component which is a rank one matrix and use the product of two singular vectors derived from the nonlinear carrier function to fit it. Finally, the fitted first dominant component is employed to compensate the nonlinear carrier phase left by the spectral translation. The proposed method has several advantages. Firstly, it is fully automatic and demands less human intervention because no data points need to be collected from the reference plane in advance. Then, it is efficient as only a single fringe pattern is required to remove the nonlinear carrier phase, which indicates its applicability to the measurement of moving objects. Lastly, the image distortion correction is performed on the captured fringe pattern, thus reducing the measurement error. Our experiments verify that the proposed technique is able to remove the carrier phase effectively in both static and dynamic measurements.

2. Principle

A typical arrangement of a divergent fringe projection measurement system is shown in Fig. 1. A straight and equally spaced fringe pattern is projected onto the tested object by a projector and then captured by a CCD camera at a different angle. It can be seen that due to the inherent nature of the divergent projection the fringes in the captured image are no long uniformly distributed as they would become much wider when they get close to the left. In the Fourier transform profilometry, the captured fringe image can be represented by

$$I(j,k)=\sum_{n=-\infty}^{+\infty}A_n r(j,k)\exp\{i[n\phi_{carri}(j)+n\phi_{obj}(j,k)]\} \tag{1}$$

where (j,k) is the pixel coordinate, r is the distribution of the reflectivity, A_n being the weighting factors of the Fourier series, ϕ_{carri} and ϕ_{obj} the phase of the carrier and the tested object. After the Fourier transform, extracting the first order term of the Fourier spectra and the inverse Fourier transform, we will have

$$I_F(j,k)=A_1 r(j,k)\exp\{i[\phi_{carri}(j)+\phi_{obj}(j,k)]\} \tag{2}$$

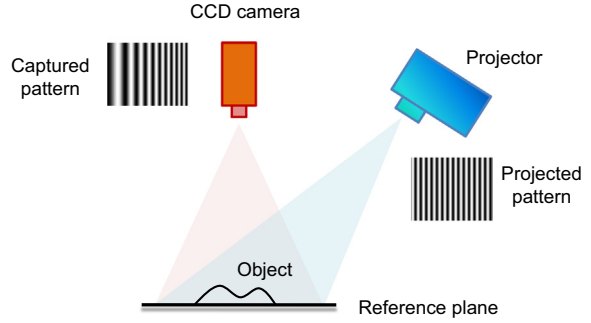

Fig. 1. Schematic experimental arrangement of a divergent fringe projection system.

To derive the carrier phase, the schematic geometry of the measurement system is illustrated in Fig. 2. Point O serves as the point light source of the projector and it has a distance h_0 from the reference plane. The dot-dashed line OC shows the projection direction at an angle of θ. Equally spaced grating FH, which is perpendicular to the projection direction, is projected divergently to the reference plane. Line OD is an arbitrary light beam with an angle α that meets the reference plane at point D. Lines DK and AE are set to be parallel to FH for the derivation of the fringe pitch on the reference plane. As the fringe pitch p_{DK} on the line DK is uniform, it can be written as

$$p_{DK}=p_{FH}\frac{x\ \sin\ \theta+l_{OB}}{l_{OG}} \tag{3}$$

where p_{FH} is the fringe pitch in FH, x being the distance from the starting point E to the point D and l the length of the line segment. In the close region of point D shown in the enlarged view, assuming the angle α to be constant yields

$$p(x)=p_{DK}\frac{\sin\ [\pi-(\pi/2-\alpha)-\theta]}{\sin(\pi/2-\alpha)}=p_{DK}\frac{\cos(\alpha-\theta)}{\cos\ \alpha} \tag{4}$$

where $p(x)$ is the fringe pitch at point D.

Since the relationships $\cos\ \alpha=h_0/\sqrt{h_0^2+(x+L_0)^2}$, $\tan\ \alpha=(x+L_0)/h_0$ and $l_{OB}=h_0\ \cos\ \theta+L_0\ \sin\ \theta$ can be easily found, Eq. (4) can be further expressed as

$$p(x)=p_{DK}\frac{(l_{OB}+x\ \sin\ \theta)^2}{h_0 l_{OG}} \tag{5}$$

Thus, the carrier phase on the reference plane is given by

$$\phi_{carri}(x)=\phi_E+\int_0^x\frac{2\pi}{p(u)}du \tag{6}$$

where ϕ_E is the carrier phase at the starting point. Referring to [19], the integral term $\int_0^x 2\pi/p(u)du$ can be represented as a series when $l_{OB}>x\ \sin\ \theta$. Hence, the carrier phase in Eq. (6) can be further simplified as

$$\phi_{carri}(x)=\sum_{n=0}^{\infty}a_n x^n \tag{7}$$

where a_n is the coefficient to be estimated. Practically, because it is difficult to ensure that all the fringes are strictly vertical which

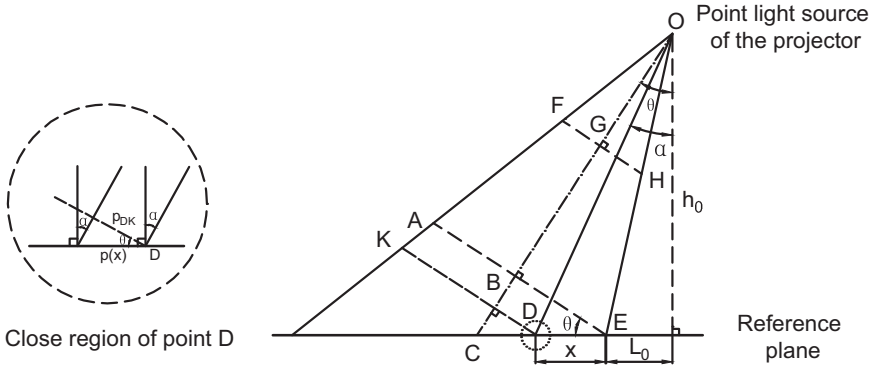

Fig. 2. Geometry of the measurement system.

means the fringes are tilted, the carrier phase in the above equation is required to add additional vertical terms with respect to y direction:

$$\phi_{carri}(x,y)=\sum_{n=0}^{\infty}a_n x^n+\sum_{n=0}^{\infty}b_n y^n \tag{8}$$

Traditionally, the method of spectra translation is used to remove the carrier phase:

$$\phi'_{carri}(x,y)=\sum_{n=0}^{\infty}a_n x^n+\sum_{n=0}^{\infty}b_n y^n-cx-dy=\sum_{n=0}^{\infty}e_n x^n+\sum_{n=0}^{\infty}f_n y^n \tag{9}$$

$$I'_F(x,y)=A_1 r(x,y)\exp\{i[\phi'_{carri}(x,y)+\phi_{obj}(x,y)]\} \tag{10}$$

where ϕ'_{carri} and I'_F are the carrier phase and image after spectra translation. It is obvious that by the way of spectra translation the carrier phase has not been removed completely as there still exist some remaining carrier terms, which can also be written in series. Thus to cope with the problem, the proposed method resorts to the principal component analysis.

As the term $\exp[i\phi'_{carri}(x,y)]$ can be expressed as

$$\exp[i\phi'_{carri}(x,y)]=\exp\left[i\left(\sum_{n=0}^{\infty}e_n x^n\right)\right]\exp\left[i\left(\sum_{n=0}^{\infty}f_n y^n\right)\right] \tag{11}$$

We find that this term is actually a rank one matrix, which can be represented by the multiplication of the two vectors $u(x)=\exp[i(\sum_{n=0}^{\infty}e_n x^n)]$ and $v(y)=\exp[i(\sum_{n=0}^{\infty}f_n y^n)]$ as

$$\exp[i\phi'_{carri}(x,y)]=v(y)u^*(x) \tag{12}$$

where $u^*(x)$ represents the conjugate transpose of $u(x)$. Generally, the nonlinear carrier would account for a large amount of region in the measured scene which means the proportion of the phase of the carrier is much larger than that of phase of the object to the whole measured area. Thus the object phase distributing in a relative small area can be assumed as a small perturbation to the overall retrieved phase, leading to the result that the first principal component approximation (*FPCA*) of the whole phase map will correspond to the carrier phase component rather than the object phase. Therefore, we will have

$$C=FPCA(\exp\{i[\phi'_{carri}(x,y)+\phi_{obj}(x,y)]\})=\exp[i\phi'_{carri}(x,y)] \tag{13}$$

$$\phi_C=\phi'_{carri}(x,y)=\sum_{n=0}^{\infty}e_n x^n+\sum_{n=0}^{\infty}f_n y^n \tag{14}$$

where C is the first principal component of the exponential form of the phase map after spectral translation and ϕ_C the phase map of the first principal component C. To perform the PCA, one can use the singular value decomposition (SVD) that is given as follows:

$$\exp\{i[\phi'_{carri}(x,y)+\phi_{obj}(x,y)]\}=V\sum U^* \tag{15}$$

where $\sum$ is an $m\times n$ rectangular diagonal matrix with non-negative real numbers on the diagonal, V and U are unitary matrixes with size of $m\times m$ and $n\times n$ respectively. Then to calculate the coefficients e_n and f_n, we conduct the following polynomial fittings:

$$P[v(y)]=fit\{unwrap[P(V_{1st\_col})]\} \tag{16}$$

$$P[u(x)]=fit\{unwrap[P(U_{1st\_col})]\} \tag{17}$$

where subscript $1st\_col$ represents taking the first column of a matrix, P is to compute the phase value and *unwrap* means to apply the phase unwrapping to the solved phase. It should be noted that polynomial fittings are used to constrain the phase distribution in both x and y directions. Because the solved first principal component by Eq. (15) will involve partial object phase due to the presence of the object. Thus to reduce the effect, the raw phase components are required to be fitted according to the ideal carrier phase distributions along the two directions.

Because the coefficients in ϕ'_{carri} have been determined, the conjugate term $\exp[-i\phi'_{carri}(x)]$ can then be multiplied with the

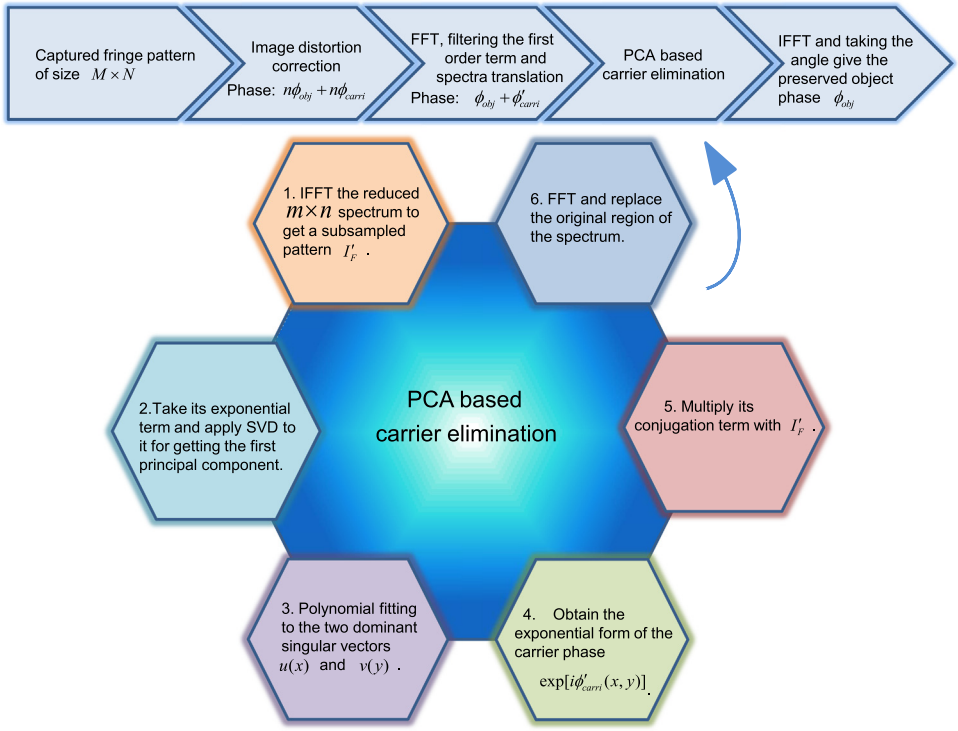

Fig. 3. Flow chart of the proposed method.

image I'_F to eliminate the remainder carrier

$$\exp[-i\phi'_{carri}(x,y)]I'_F(x,y) = A_1 r(x,y)\exp[i\phi_{obj}(x,y)] \quad (18)$$

It should be noted that to improve the precision of the proposed method, the image distortion correction is required to carry out to deal with the captured image. Further, to lower the computational complexity, the present method is conducted only within a reduced $m \times n$ spectrum area of the whole $M \times N$ region. This action will largely boosts the computational speed while do not compromise the accuracy because once the fringe image is filtered, the complex field is oversampled. Fig. 3 shows the flow chart of the proposed method.

3. Experiments

A divergent fringe projection system composed of an industrial CCD camera (GE680) with maximum frame rate of 205, the DLP Light Crafter DMD kit and a data processing device (Dell OptiPlex 990) has been developed. Three experiments have been conducted to demonstrate the practicability of the proposed method. The first

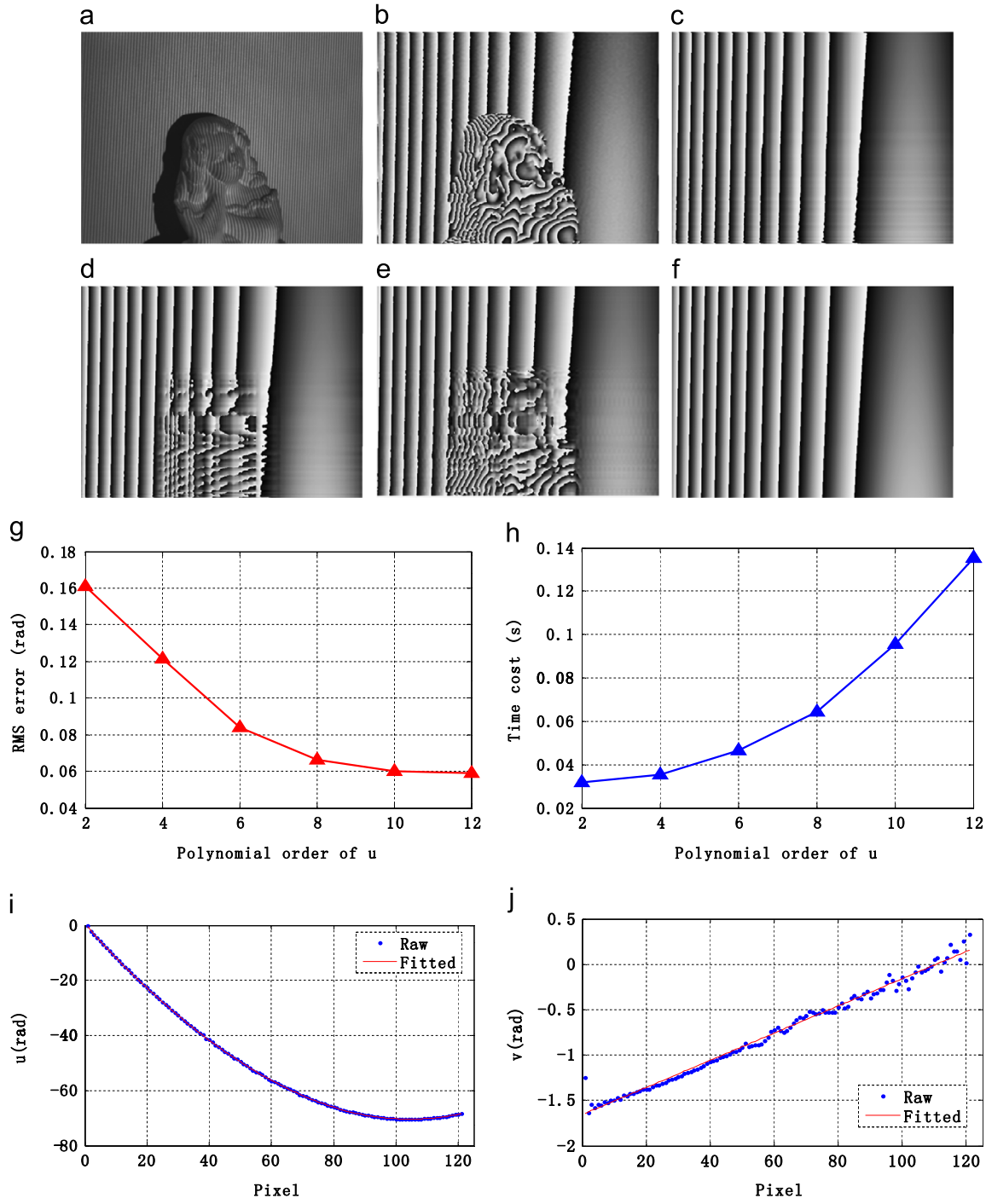

Fig. 4. Experimental images of the static measurement. (a) Fringe pattern cast on a plaster model; (b) phase map obtained by the spectral translation; (c) the raw carrier phase formed from the first dominant singular vectors; (d) and (e) demonstrate the phase reconstructed from the first two and five dominant components, respectively; (f) phase map of the fitted first dominant component; (g) RMS error with different polynomial order of u; (h) time cost for the different polynomial order of u; (i) and (j) show the two unwrapped first dominant singular vectors and the corresponding fitted results.

one intends to show the technique's performance for static scene measurement, the second exams its accuracy and the last one demonstrates its applicability in dynamic measurement. The used camera has been calibrated for the image distortion correction.

In Fig. 4(a), a static plaster model was measured. After performing the Fourier transform, a rectangular window of size 121×121 was applied to filter the $+1$ order spectrum. Then translating the maximum of the filtered spectrum to the center of the whole spectrum and implementing the inverse Fourier transform, the reconstructed wrapped phase was obtained and shown in Fig. 4(b). It can be seen that the spectral translation did not remove the carrier completely as some nonlinear phase components can still be observed clearly in the background. So to compensate the remaining carrier phase, the proposed method was applied. The inverse Fourier transform was applied to the filtered spectrum with dimension 121×121 and the exponential form of the resultant phase was analyzed by the PCA. Fig. 4(c) shows the raw carrier phase from the first principal component obtained. We found that nearly all the remaining nonlinear phase components were separated from the object phase. Fig. 4(d) and (e) shows that the object phase is emerging gradually when the phase is reconstructed by the first two and the first five dominant components. Then the phases of the two dominant singular vectors of the first dominant component were unwrapped, and they were to be fitted by the polynomial fitting. Since the fringe pattern was vertically projected and slightly tilted, the variation of phase in y direction could be treated as linear. Thus the 1st order polynomial function would be adequate to fit v. To determine the proper polynomial order of u, we chose different orders of u to conduct the experiment to see their performances. Fig. 4(g) and (h) shows the root mean square (RMS) error of the measured results and the time cost with various orders of u, respectively. From Fig. 4(g), it can be seen that the error is decreasing as the higher order is used to fit u and when the order is larger than eight, the higher order contributes little to the measurement accuracy. From Fig. 4(h), the time cost keeps rising as the polynomial fitting of higher order is conducted. Since the accuracy is not to be improved significantly and the computational time is going to increase rapidly as more than eight order polynomial fitting is used, we chose the 8th order polynomial function to fit the vector u in our measurement. The fitting results are shown in Fig. 4(i) and (j). The final computed nonlinear carrier phase with smoother phase distribution is demonstrated in Fig. 4(f). By the comparison of Fig. 4(c) and (f), we find that although the raw carrier phase was slightly damaged by the object phase, this influence can then be eliminated by the employment of the polynomial fittings. After applying the fitted carrier phase to Fig. 4(b) for compensation, the result is shown in Fig. 5(a). Through performing the phase unwrapping and removing some unreliable regions, i.e. the shadows, we got the final unwrapped phase shown in

Table 1
Error comparison of spectral translation method and the proposed method.

	Spectral translation method	Proposed method
Average error (rad)	6.586	0.095
RMS (rad)	5.999	0.066

Table 2
Computational time of the proposed method.

	Time cost (s)
PCA (SVD)	0.0270
Polynomial fitting	0.0743
Compensation	0.0325
Total	0.1338

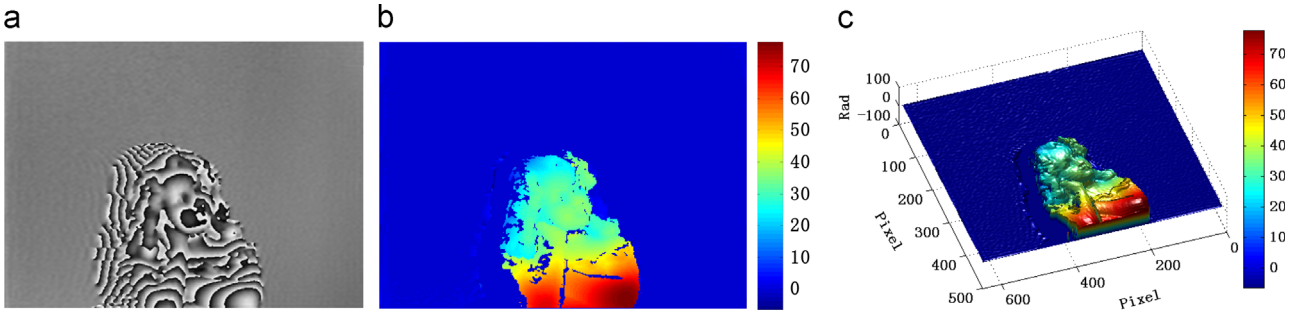

Fig. 5. Measurement results of the first experiment. (a) Wrapped phase map after the compensation of the nonlinear carrier; (b) and (c) demonstrate the corresponding unwrapped phase viewed from the front and the side, respectively.

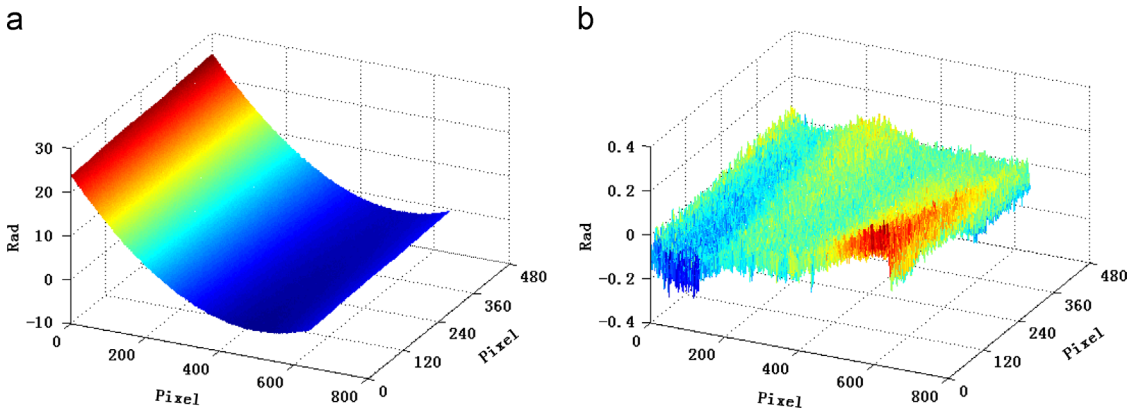

Fig. 6. Error comparison of the spectral translation method and the proposed method. (a) Error of the spectral translation method; (b) error of the presented method.

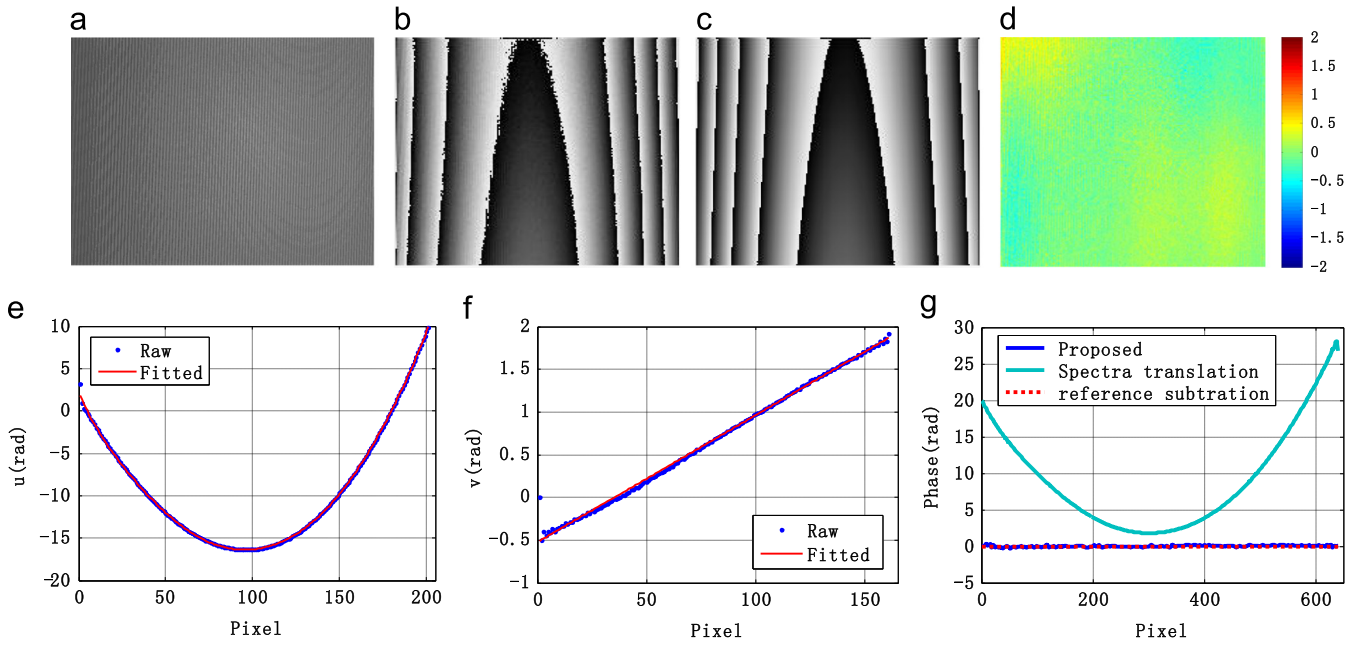

Fig. 7. Accuracy examination. (a) Fringe pattern projected onto a flat surface; (b) phase map reconstructed through the spectral translation method; (c) phase distribution obtain from the fitted first dominant component; (d) the measured phase of the surface by the proposed method; (e) and (f) show the two unwrapped singular vectors of the first dominant component and their corresponding fitted results; (g) comparisons of the results obtained from different techniques.

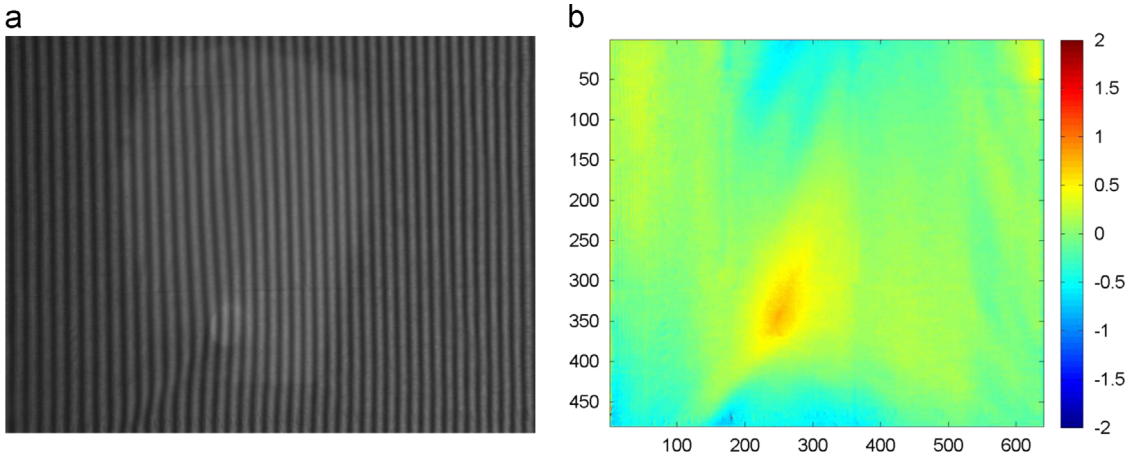

Fig. 8. Experiment of a dynamic scene. (a) One of the captured fringe images; (b) the corresponding reconstructed phase distribution.

Fig. 5(b) and (c). During the whole process, the nonlinear carrier was determined automatically only by the captured fringe image and no human intervention was involved. To see the effectiveness of the proposed method, we compared the error of the spectral translation method and the proposed method. Fig. 6 and Table 1 are the error distribution and the corresponding error data, respectively. For the error analysis, the retrieved phase of the reference subtraction approach was employed to be the natural phase of the object. It can be seen that the error can be greatly reduced by the proposed method and it will be a good alternative when extra measurement of the reference subtraction method is not available. Moreover, the computational time of the presented method is also given in Table 2. The whole processing time is only 0.1338 s using a computer of 2.8 GHz, which shows our method is of high efficiency.

In the second experiment, we examined the accuracy of the presented technique. Fig. 7(a) shows the tested flat surface and theoretically its measured phase should be zero. After filtering the first order spectrum with windows size of 161×201 and spectral translation, the reconstructed wrapped phase was obtained and shown in Fig. 7(b). Then carry out the inverse Fourier transform to handle the cropped spectrum and analyze the exponential term of the subsampled complex field with PCA. Fig. 7(e) and (f) demonstrates the fitting results of the two dominant singular vectors u and v. The nonlinear phase distribution calculated from the fitted first dominant component is acquired and shown in Fig. 7(c). After compensation and phase unwrapping, the final phase of the flat surface is shown in Fig. 7(d) where the average phase of the whole surface is -0.0074 rad with RMS error of 0.0029 rad. Further, in Fig. 7(g) we plotted the 240th row of the measured scene and compared our result with the one without compensation and the one from method of reference subtraction which is the most robust one among the existing carrier removing methods [20]. It can be seen that shown by the curve the solved phase was nonlinearly distributed without the compensation. After using the proposed method to compensate the nonlinear phase, the curve was changed into a straight line which is very close to the result from the reference subtraction technique, indicating that our method is a good alternative for the carrier elimination. By the

proposed method, the average phase of the row is 0.0081 rad with RMS error of 0.0052 rad. The experiment verifies that the proposed method is capable of compensating the nonlinear carrier phase accurately.

Lastly, a dynamic measurement was conducted. Here, a tissue was pasted to a flat and hollow surface. A pen was pushing the tissue from its back and meanwhile kept doing circular motions. The camera–projector pair was running at 120 Hz. The dynamic process was captured and saved, and subsequently handled with our method. Fig. 8(a) shows one frame of the measured scene and Fig. 8(b) the corresponding solved phase distribution. The experimental video is presented where a small patch caused by the push shows a local bump and the rest region remains almost flat. The experiment reveals that the developed technique can successfully eliminate the carrier phase for the dynamic measurement.

Supplementary material related to this article can be found online at doi:10.1016/j.optlaseng.2015.05.009.

4. Conclusion

In this work, a new method based on PCA is proposed to remove the carrier phase in FTP. Applying the PCA to the exponential form of the resultant phase by the spectral translation, the obtained first dominant component contains all of the nonlinear phase to be removed. Then the dominant component is refined by the multiplication of the two fitted singular vectors based on the derived carrier phase function with the goal of reducing the effect of the object phase involved in the solved first principal component. Lastly, the nonlinear carrier phase left by the spectral translation is compensated with the phase of the refined first dominant component. The proposed method is efficient and automatic since only one fringe pattern is required to eliminate the carrier and during which no human intervention is needed. Further, the influence of the image distortion is removed, ensuring the measurement with high accuracy. It should be noted that as we assume the object phase to be a small perturbation to the overall retrieved phase, it is better to leave sufficient region for the reference plane in the measured scene. This will help the PCA to automatically identify the carrier phase from the whole phase map. The proposed method is able to facilitate the process of the carrier removal and reduce the complexity of the experiment compared to the existing techniques. Although the phase-to-height conversion is not addressed directly by the proposed method, it could bring benefits to the system calibration because the phase-height relationship would become linear due to the removal of the nonlinear carrier. In conclusion, the proposed technique allows accurate and automatic carrier removal for both static and dynamic measurements.

References

[1] Chen F, Brown GM, Song M. Overview of three-dimensional shape measurement using optical methods. Opt Eng 2000;39:13.
[2] Gorthi SS, Rastogi P. Fringe projection techniques: whither we are? Opt Lasers Eng 2010;48:18.
[3] Chen L, Quan C, Tay CJ, Fu Y. Shape measurement using one frame projected sawtooth fringe pattern. Opt Commun 2005;246:10.
[4] Huang L, Ng CS, Asundi AK. Fast full-field out-of-plane deformation measurement using fringe reflectometry. Opt Lasers Eng 2012;50:4.
[5] Zuo C, Chen Q, Gu G, Feng S, Feng F, Li R, et al. High-speed three-dimensional shape measurement for dynamic scenes using bi-frequency tripolar pulse-width-modulation fringe projection. Opt Lasers Eng 2013;51:8.
[6] Feng S, Zhang Y, Chen Q, Zuo C, Li R, Shen G. General solution for high dynamic range three-dimensional shape measurement using fringe projection technique. Opt Lasers Eng 2014.
[7] Zhang S. Recent progresses on real-time 3D shape measurement using digital fringe projection techniques. Opt Lasers Eng 2010;48:11.
[8] Su X, Zhang Q. Dynamic 3-D shape measurement method: a review. Opt Lasers Eng 2010;48:14.
[9] Zhang Q, Su X. High-speed optical measurement for the drumhead vibration. Opt Express 2005;13:7.
[10] Zhang Q, Su X, Cao Y, Li Y, Xiang L, Chen W. Optical 3-D shape and deformation measurement of rotating blades using stroboscopic structured illumination. Opt Eng 2005;44:7.
[11] Huang L, Kemao Q, Pan B, Asundi AK. Comparison of Fourier transform, windowed Fourier transform, and wavelet transform methods for phase extraction from a single fringe pattern in fringe projection profilometry. Opt Las Eng 2010;48:8.
[12] Zuo C, Chen Q, Gu G, Feng S, Feng F. High-speed three-dimensional profilometry for multiple objects with complex shapes. Opt Express 2012;20:18.
[13] Feng S, Chen Q, Zuo C, Sun J, Yu S. High-speed real-time 3-D coordinates measurement based on fringe projection profilometry considering camera lens distortion. Opt Commun 2014;329:14.
[14] Zhang S. High-resolution, real-time three-dimensional shape measurement. Opt Eng 2006;45:8.
[15] Huang L, Ng CS, Asundi AK. Dynamic three-dimensional sensing for specular surface with monoscopic fringe reflectometry. Opt Express 2011;19:6.
[16] Takeda M, Ina H, Kobayashi S. Fourier-transform method of fringe-pattern analysis for computer-based topography and interferometry. J Opt Soc Am 1982;72:5.
[17] Takeda M, Mutoh K. Fourier transform profilometry for the automatic measurement of 3-D object shape. Appl Opt 1983;22:6.
[18] Chen L, Quan C. Fringe projection profilometry with nonparallel illumination: a least-squares approach. Opt Lett 2005;30:3.
[19] Chen L, Tay CJ. Carrier phase component removal: a generalized least-squares approach. J Opt Soc Am A 2006;23:9.
[20] Zhang Q, Wu Zhiyun. A carrier removal method in Fourier transform profilometry with Zernike polynomials. Opt Lasers Eng 2013;51:8.
[21] Zuo C, Chen Q, Qu W, Asundi A. Phase aberration compensation in digital holographic microscopy based on principal component analysis. Opt Lett 2013;38:3.